Available online at www.sciencedirect.com

ScienceDirect

journal homepage: www.elsevier.com/locate/issn/15375110

Research Paper

An evaluation of a vision-based sensor performance in Huanglongbing disease identification

Alireza Pourreza [a], Won Suk Lee [a,*], Ed Etxeberria [b], Arunava Banerjee [c]

[a] Department of Agricultural and Biological Engineering, University of Florida, Gainesville, FL, USA
[b] Department of Horticultural Sciences, University of Florida/IFAS, Citrus Research and Education Center, Lake Alfred, FL, USA
[c] Department of Computer and Information Science and Engineering, University of Florida, Gainesville, FL, USA

ARTICLE INFO

Article history:
Received 14 August 2014
Received in revised form
11 November 2014
Accepted 25 November 2014
Published online 18 December 2014

Keywords:
Citrus disease
Huanglongbing
Image analysis
Starch
Vision sensor

Huanglongbing (HLB) disease is a critical infection which has dangerously affected the citrus production in Florida and has also been observed in California and Texas. No active treatment for this infection has been reported yet and the HLB infected tree will eventually die. However, early identification and removal of the HLB affected trees will secure the healthy trees in the grove. Accumulation of starch on infected leaves is an early symptom of HLB. Starch can rotate the polarisation plane of light in a certain waveband. A customised vision sensor was developed based on this characteristic to identify the HLB symptom. The vision sensor images were compared with the images captured by a colour camera to demonstrate the improvement achieved in this method. Also, the starch accumulation identification was studied for citrus leaves before and after being ground. The results showed an enhanced HLB identification performance using the developed vision sensor.

© 2014 IAgrE. Published by Elsevier Ltd. All rights reserved.

1. Introduction

Huanglongbing (HLB), also called "citrus greening" or "yellow shoot disease", is an extremely lethal infection of citrus trees first discovered in 2004 on the American continent in Brazil (Halbert, 2005), and later in Florida in August 2005 (Texeira et al., 2005). Shortly after, HLB infection spread over the entire state of Florida and is now present in Texas (Kunta et al., 2012), and California (Kumagai et al., 2014). Presently, there are no effective treatments and infected trees will eventually die after a few years. Nevertheless, early HLB detection and removal of the infected trees will prevent other healthy trees in the grove from acquiring the disease. Common symptoms of HLB are chlorosis and mottling of the leaves, uneven fruit colouring, and unevenly shaped and

* *Corresponding author*. 207 Frazier Rogers Hall, PO Box 110570, Gainesville, FL 32611, USA. Tel.: +1 352 392 1864x207; fax: +1 352 392 4092.
E-mail addresses: apourreza@ufl.edu (A. Pourreza), wslee@ufl.edu, wlee32608@gmail.com (W.S. Lee), eetxeber@ufl.edu (E. Etxeberria), arunava@cise.ufl.edu (A. Banerjee).
http://dx.doi.org/10.1016/j.biosystemseng.2014.11.013
1537-5110/© 2014 IAgrE. Published by Elsevier Ltd. All rights reserved.

bitter tasting fruit. The yellowish/blotchy symptom of HLB-infected leaves resembles that of some nutrient deficiencies (especially zinc deficiency), making it difficult to distinguish from such deficiencies. Additional molecular analysis is usually required for an accurate diagnosis (Albrecht & Bowman, 2008). However, HLB leaf symptomatology develops from the accumulation of starch in the leaf tissue, a property that can be exploited for diagnostic means (Takushi et al., 2007).

Futch, Weingarten, and Irey (2009) showed that the accuracy of a human-based HLB diagnosis by visual inspection would not be greater than 59%. Gonzalez, Reyes-De-Corcuera, and Etxeberria (2012) showed that the level of starch in a citrus leaf can be measured in a laboratory to expose its HLB status. However, qrt-PCR test was reported as the most accurate laboratory-based HLB diagnosis method (Hansen, Trumble, Stouthamer, & Paine, 2008). Although both the qrt-PCR and the starch measurement methods are comparatively accurate, they need sample collection and preparation which are extremely time-consuming and labour-intensive, and cannot be employed for constant grove monitoring.

Spectroscopy methods have been widely used by researchers for plant status monitoring (Xie, Li, Nie, & He, 2013). Mishra, Ehsani, Albrigo, and Lee (2007) evaluated the capability of near-infrared, red, and green spectral bands in HLB identification. Later, they designed an optical sensor with the ability to measure the citrus trees' reflectance at 970 nm, 870 nm, 670 nm, and 570 nm. Using this sensor, they realised that they can achieved an accuracy of over 95% if the tree's reflectance is measured multiple times (Mishra, Karimi, Ehsani, & Albrigo, 2011). The mid-infrared band was found to have potential to determine the HLB status of ground citrus leaves (Hawkins et al., 2010). Sankaran, Ehsani, and Etxeberria (2010) showed that the reflection of a ground citrus leaf in mid-infrared band could identify not only its HLB status, but also its nutrient deficiency status with an accuracy of over 90%. It was shown in another study that aside from HLB and nutrient deficiency status, other citrus diseases could also be identified by analysing the ground leaf's reflection in the near-infrared, with true positive rates between 92% and 99% (Windham et al., 2011).

Kim et al. (2009) analysed digital microscopic images of citrus leaves to classify them into several classes including two HLB, two healthy, and three nutrient deficiency classes. They achieved an overall accuracy of 87% using the textural descriptors extracted from the images.

Li, Lee, Wang, Ehsani, and Yang (2012) also employed airborne multispectral (MS) and hyperspectral (HS) images to identify the HLB infected areas in the grove. Li, Lee, Li, et al. (2012) compared different airborne MS and HS image analysis methods for HLB detection. They showed that the spectral information divergence (SID) method had the best accuracy. Later Li, Lee, Wang, Ehsani, and Yang (2014) employed an spectral angle mapping (SAM) method and their extended approach resulted in an accuracy of 86% for HLB detection. In another study, images acquired by a multiband imaging sensor mounted on an UAV (six-rotor helicopter) were used to detect HLB infected trees. Accuracies ranging from 67% to 85% were achieved in HLB infection identification using this method (Garcia-Ruiz et al., 2013).

It was shown in our previous study (Pourreza, Lee, Raveh, Ehsani, & Etxeberria, 2014) that the unique starch characteristic of rotating the polarisation plane of light can be effectively used in identification of starch accumulation in an HLB infected citrus leaf. A customised image acquisition system was developed for this purpose and it was able to clearly highlight the HLB infected areas on citrus leaves; however, its HLB detection accuracy within the zinc deficient samples was not as good. In this study, another vision sensor was developed to improve the efficiency of the first prototype and add more capabilities. The main objective of this study was to evaluate the HLB identification performance of the proposed vision sensor and confirm its efficiency. The specific goals were to (1) assess the improvement in HLB identification achieved by using narrow band illumination and polarising filters in comparison with a natural imaging condition, and (2) compare the effect of starch accumulation on the images of citrus leaves before and after being ground.

2. Materials and methods

2.1. Data collection

Two sample sets of Hamlin sweet orange leaves were collected from citrus trees at the Citrus Research and Education Center (CREC), University of Florida (Lake Alfred, Florida). There were 60 citrus leaves in the first sample set of 20 HLB-positive, 20 HLB-negative, 10 zinc-deficient HLB-positive, and 10 zinc-deficient HLB-negative samples. This sample set was used for comparing the images acquired by the proposed vision sensor with the images of the same samples that were obtained with another colour camera. The second sample set included another 30 samples, of 10 HLB-positive, 10 HLB-negative, 7 zinc-deficient HLB-positive, and 3 zinc-deficient HLB-negative. The second sample set was created to compare the images of the samples with the images of the same leaves after grinding. A qrt-PCR examination (Hansen et al., 2008) was performed on all the 90 samples in both sample sets to confirm the HLB status of the leaves. The qrt-PCR test was done in the U.S. Sugar Corporation's Southern Gardens processing plant (Clewiston, FL).

2.2. Image acquisition

According to the results of the previous study (Pourreza, Lee, Raveh, Hong, & Kim, 2013), starch in the HLB infected leaf was able to rotate the light polarisation mainly around 600 nm. These results were used to develop a vision-based sensor with the ability to highlight the symptomatic areas on an HLB infected leaf which contained excessive amount of starch. The vision sensor included a monochrome camera (DMK 23G445, TheImagingSource, Bremen, Germany) with high sensitivity at 591 nm, and 10 high power (10 W) narrow band LEDs (LS4-00A100, LED Engin, San Jose, California) concentrated at 591 nm which were mounted in a 13 × 19 × 15 cm wooden box (Fig. 1). Five LED drivers (RCD-48, RECOM, Brooklyn, New York) were used to power the LEDs. A wide lens with a 6 mm focal length was used for the camera to maximise its depth of field. Also one linear polariser was

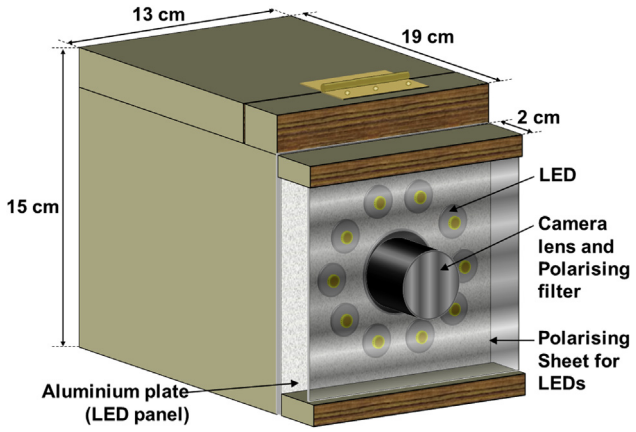

Fig. 1 – Image acquisition system including the camera, lens, polarising filters and LED panel enclosed in a wooden box.

installed in front of the camera's lens, and another polarising film (visible linear polarising laminated film, Edmund Optics, Barrington, New Jersey) with a perpendicular direction to the camera's filter was fixed in front of the LED panel (Fig. 1). Using this setting, the camera only receives the minimum reflection.

2.3. Imaging conditions evaluation

Images of citrus leaves in the first sample set were acquired with the vision sensor in a completely dark room from a distance of 80 cm because the minimum number of saturated pixels were achieved at this distance while pixel values were well distributed within the entire dynamic range. Therefore, the leaf samples only received the narrow band polarised light produced by the sensor. In order to evaluate the HLB identification efficiency of the sensor, another set of images from the same sample set were created using an RGB camera (EOS Rebel T2i, Canon, Tokyo, Japan) and with common indoor fluorescent light. All the RGB images were captured in the manual mode with a shutter speed of 0.04 s, a focal ratio of F4.5, and sensitivity of ISO800 to confirm the imaging condition uniformity and prevent the effect of camera settings on the evaluation results. The histograms of the red, green, blue, and grey (average of red, green, and blue) components of the RGB colour space and relative luminance (Y), blue-difference (Cb), and red-difference (Cr) components of YCbCr colour space were extracted from the symptomatic areas on each leaf and compared to the same symptomatic areas on the images captured by the vision sensor. Also mean and standard deviation features of the leaf area were extracted from the vision sensor images and the six colour components of the colour images, to visualise the samples in a 2-dimensional space and evaluate the separability of the four classes of HLB-positive, zinc-deficient HLB-positive, zinc-deficient HLB-negative, and HLB-negative leaves. A maximum margin approach (Bishop, 2006) was employed to determine the optimum thresholds between each pair of classes for the scatter plot of the samples images acquired by the vision sensor.

2.4. Discriminant analysis

In order to compare the separability of the four classes in the two imaging conditions, Fisher ratio was used as the separability index and it was calculated using the features extracted from the vision sensor images and all seven components of the RGB images (red, green, blue, grey, Y, Cb, Cr). Fisher ratio defines the ratio of the between-class variability to the within-class difference (Han, Lee, & Bien, 2013). Equation (1) shows the Fisher ratio for one feature in a 2-class problem.

$$F_{ij} = \frac{\left(\mu_i - \mu_j\right)^2}{\left(\sigma_i^2 + \sigma_j^2\right)} \tag{1}$$

where μ_i and μ_j are the means and σ_i and σ_j are the standard deviations in class i and j. F_{ij} shows the degree of the class separability in the direction of the corresponding feature. However, in order to improve the identification accuracy, two features (grey values' mean and standard deviation) were employed in this experiment and the effect of the two on a single separability index was needed. Therefore, a Fisher's linear discriminant analysis (LDA) was used to reduce the dimension of the feature vector to one dimensional for each pair of classes (Bishop, 2006) and then the Fisher ratio was calculated for the corresponding pair of classes. In Fisher's LDA (equation (2)), a function is employed to project the vector x down to a one-dimension vector (y).

$$y = w^T x \tag{2}$$

The projection method in Fisher's LDA was employed because it optimises the weight vector (w) by maximising the separation between the projected classes and minimising variation within each projected class (equation (3)).

$$w \propto S_W^{-1}(m_2 - m_1) \tag{3}$$

where S_W is the total within class covariance matrix, and m_1 and m_2 are the means of class one and two respectively. Using this projection, the Fisher ratio was computed between each pair of classes; however, the dataset included four classes and consequently a single separability index was required to describe the separability for all four classes. For this purpose, the arithmetic average of Fisher ratios for all possible pairs of classes was computed (equation (4)) and considered as the general separability index (F) for comparison of HLB identification efficiencies between the sensor images and the RGB images.

$$F = \frac{\sum_{i}^{C}\sum_{j}^{C} P_i P_j F_{ij}}{C(C-1)\sum_{i}^{C}\sum_{j}^{C} P_i P_j} \tag{4}$$

where P_i and P_j are proportional to the number of samples in classes i and j, and C indicates the number of classes.

2.5. Sample condition evaluation

In this part, the images of the leaves in the second sample set were compared to the same samples after being ground, to

Table 1 – The cycle threshold (CT) values measured for the citrus leaves in the first sample set.

HLB Negative				HLB-positive				Zn Def. HLB-negative				Zn Def. HLB-positive			
ID	CT Value	μ[a]	σ[b]	ID	CT Value	μ	σ	ID	CT Value	μ	σ	ID	CT Value	μ	σ
21	40.0	38.3	5.7	41	28.0	48.5	14.8	1	40.0	84.7	65.8	2	24.9	100.4	42.6
22	40.0	28.4	4.2	42	23.2	51.5	14.9	3	37.7	110.3	65.7	6	23.3	114.8	37.1
23	40.0	49.5	8.0	43	25.4	78.7	38.9	4	40.0	89.4	58.6	8	23.6	121.0	44.1
24	40.0	26.5	3.7	44	32.3	59.7	18.8	5	40.0	107.9	58.6	9	22.6	213.8	59.0
25	40.0	20.9	4.7	45	21.9	63.8	26.9	7	40.0	121.4	85.4	11	27.8	102.9	62.4
26	40.0	26.8	4.9	46	21.5	49.3	13.6	10	40.0	127.5	77.5	13	24.6	140.9	65.7
27	40.0	28.0	3.2	47	22.3	46.2	12.7	12	40.0	119.4	82.2	14	23.2	134.5	64.3
28	40.0	26.3	4.8	48	26.5	53.4	13.5	15	40.0	98.0	55.3	18	22.1	98.7	44.5
29	40.0	23.1	3.8	49	24.4	52.2	23.7	16	40.0	128.6	69.2	19	24.3	162.1	64.5
30	40.0	23.7	3.8	50	23.1	51.8	15.6	17	40.0	89.3	63.7	20	21.4	162.3	49.7
31	40.0	35.8	4.0	51	21.9	81.2	23.0								
32	40.0	34.3	5.1	52	30.8	47.8	21.1								
33	40.0	30.2	4.8	53	24.8	56.1	18.7								
34	36.5	29.3	6.0	54	22.0	76.0	17.8								
35	40.0	33.7	4.7	55	22.7	57.5	11.0								
36	40.0	26.2	5.6	56	23.2	64.1	17.3								
37	40.0	31.9	5.3	57	26.6	69.0	15.5								
38	40.0	36.6	5.1	58	21.9	103.5	39.9								
39	40.0	41.8	4.5	59	22.8	47.8	12.1								
40	40.0	34.3	6.6	60	21.9	52.9	18.4								

[a] μ is the grey values' mean of the image captured by the vision sensor.
[b] σ is the grey values' standard deviation of the image captured by the vision sensor.

investigate whether the starch in ground infected leaves can be identified as accurately as in unground leaves. For the grinding process, the samples were first placed in a ceramic mortar and freeze-dried with liquid nitrogen (Sankaran et al., 2010) and then they were ground using a ceramic pestle. Histograms of the whole leaf area were acquired and compared with the histograms of the ground leaves. Also the grey values' means and standard deviations were extracted from both sample sets before and after being ground to visualise the samples in a 2-dimentional space. The separability indices (Fisher ratio) as explained in the previous section were calculated for comparison purposes.

All the feature extractions and analyses were conducted in MATLAB (version R2011a, MathWorks, Natick, MA), and Excel (Microsoft Office, Microsoft, Redmond, Washington) was used to visualise the samples in scatter plots.

3. Results and discussion

3.1. *Dataset validation*

The number of required cycles for the fluorescent intensity to reach the threshold is considered as the cycle threshold (CT) in a qrt-PCR test. Li, Hartung, and Levy (2006) suggested the CT value of 33 to decide about the HLB status of a sample. According to their study, a CT value smaller than 33 indicates the HLB-positive status while a CT value over 33 shows no HLB infection. The measured CT values for the citrus leaves in the first sample set are given in Table 1. Within the zinc-deficient class, 10 samples had the CT values below 33 and the rest of the samples in this class had CT values over 33. Therefore, the zinc-deficient class was divided into two subclasses of zinc-

Table 2 – The cycle threshold (CT) values measured for the citrus leaves in the second sample set.

HLB Negative				HLB-positive				Zn Def. HLB-negative				Zn Def. HLB-positive			
ID	CT Value	μ[a]	σ[b]	ID	CT Value	μ	σ	ID	CT Value	μ	σ	ID	CT Value	μ	σ
21	40.0	23.3	8.2	1	23.5	74.9	32.1	14	36.0	85.6	37.3	11	29.0	133.5	42.0
22	40.0	27.6	9.5	2	23.1	106.7	37.3	17	34.7	82.7	51.3	12	21.7	145.4	46.4
23	40.0	27.8	9.1	3	24.0	79.8	27.8	19	34.7	85.7	52.3	13	22.2	100.3	38.3
24	40.0	20.9	6.7	4	25.0	90.1	42.6					15	23.2	145.5	55.0
25	40.0	22.8	8.7	5	23.4	58.5	19.1					16	24.0	97.9	31.0
26	40.0	28.7	8.3	6	23.9	118.9	39.9					18	29.0	131.4	45.9
27	40.0	37.8	8.9	7	23.1	84.8	26.0					20	23.6	87.1	54.6
28	40.0	23.2	8.7	8	22.4	88.3	36.4								
29	40.0	27.5	9.0	9	24.4	86.5	45.1								
30	40.0	18.8	9.1	10	24.9	70.2	39.9								

[a] μ is the grey values' mean of the image captured by the vision sensor before grinding.
[b] σ is the grey values' standard deviation of the image captured by the vision asensor before grinding.

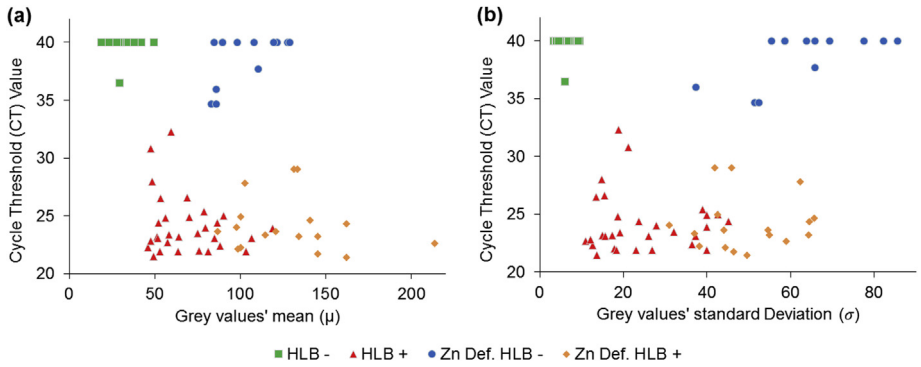

Fig. 2 – Scatter plots of samples in four classes based on their grey values features and cycle threshold (CT) values: (a) grey values' means and CTs, and (b) grey values' standard deviations and CTs.

deficient HLB-positive and zinc-deficient HLB-negative classes.

Table 2 shows the CT values for the leaves in the second sample set. Seven samples within the zinc-deficient class had CT values smaller than 33 and three zinc-deficient samples had CT values greater than 33. So they were subcategorised into zinc-deficient HLB-positive and zinc-deficient HLB-negative classes, respectively.

In order to examine the relationships between the grey value features (means and standard deviations) and CT values, two correlation analyses were conducted in MINITAB (version 15, Minitab Inc., State College, Pennsylvania). Pearson coefficients of −0.493 and −0.244 were determined for the correlations between means and CTs, and standard deviations and CTs, respectively. Since the coefficients were negative in both correlation analyses, it can be concluded that the CT values generally tended to increase as the grey value features decreased. The absolute coefficient value also tells the strength of a relationship between two variables where a perfect relationship is indicated by one, and zero means no relationship at all. Since the obtained Pearson coefficients were closer to zero than one, it can be concluded that there is no strong relationship between CT values and the grey values features. This can be also inferred from the scatter plots in Fig. 2. Basically, there is no direct correlation between degree of symptoms of a given leaf sample and its CT value. The bacteria are very unevenly distributed throughout an HLB affected tree, so variations per sample can be quite large. Additionally, HLB symptoms may show in different ways, so it is impossible to define which symptoms show up first as being correlated with CT values (Gottwald, 2010). The vision sensor in this paper was designed to highlight the accumulation of

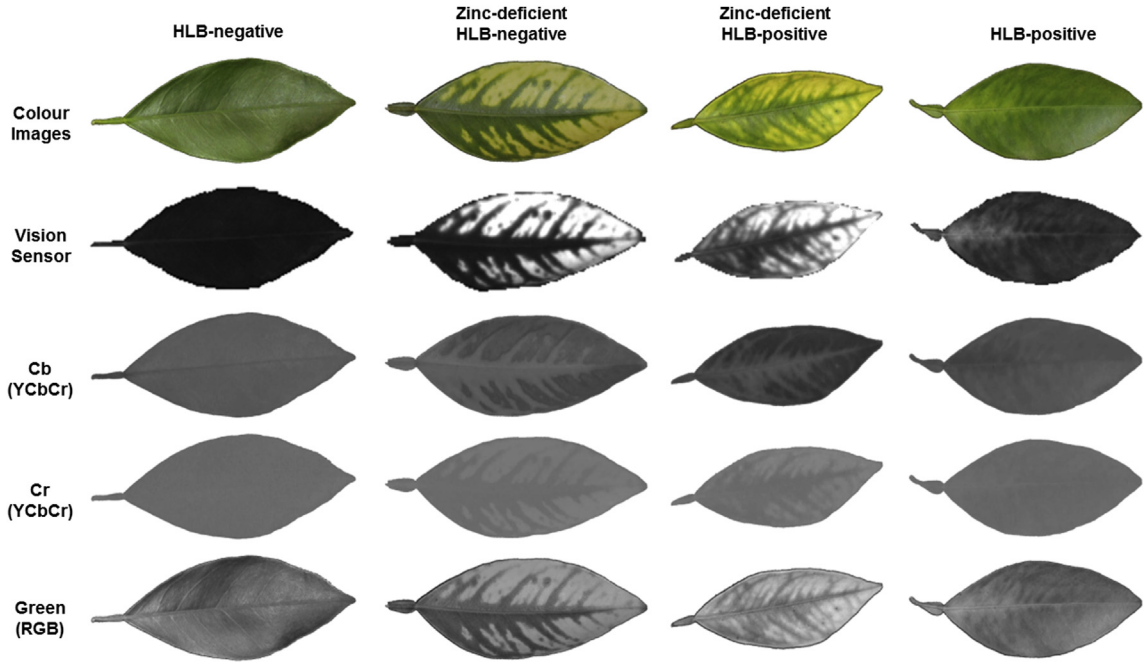

Fig. 3 – Colour photos of leaves' samples in four classes and their corresponding monochrome images captured by the vision sensor and extracted from the colour images. Cb = blue difference (YCbCr), and Cr = red difference (YCbCr). (For interpretation of the references to colour in this figure legend, the reader is referred to the web version of this article.)

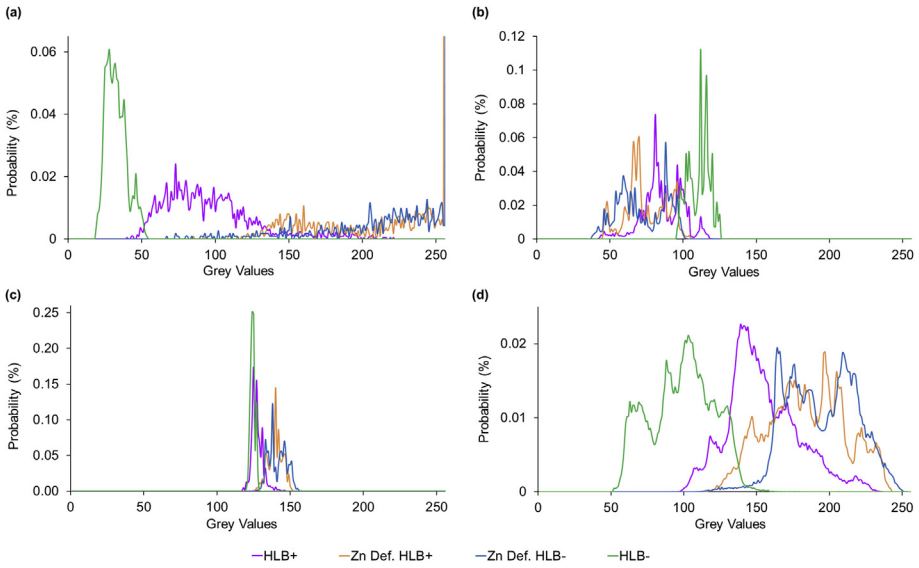

Fig. 4 – Histograms of four classes' symptomatic areas: (a) vision sensor images, (b) colour images of blue difference (Cb) component of YCbCr, (c) colour images of red difference (Cr) component of YCbCr, and (d) colour images of green component of RGB. HLB+ = infected with Huanglongbing, Zn Def. HLB+ = zinc deficient and infected with Huanglongbing, Zn Def. HLB− = zinc deficient but not infected with Huanglongbing, and HLB− = healthy.

starch; however, starch can vary drastically over a certain threshold, and it is impractical to correlate the starch accumulation to CT value in a single sample. However, the CT value can be correlated to the number of symptomatic areas on an entire tree including roots. The amount of starch accumulation indicates that HLB infection is present somewhere in the tree and this can be away from the bacterial infection, while the CT value reveals the level of infection in that particular leaf sample. As the correlation analyses confirmed, there were no strong correlations between CT values and grey values' means or standard deviations. The method presented in this paper was not meant to be quantitative in terms of bacteria but rather in terms of the presence of HLB infection in a tree.

3.2. *Comparison of imaging conditions*

Four sample images (one from each class) acquired with the vision sensor and their corresponding colour components extracted from the colour images are shown in Fig. 3. The healthy, HLB-positive, and zinc-deficient symptomatic areas appeared more distinctive in the images acquired with the vision sensor, compared to the other colour components. The separability indices (arithmetic averages of Fisher ratios) of 0.528, 0.201, 0.196, 0.136, 0.135, 0.134, 0.114, 0.003 were achieved for vision sensor, Cb component (YCbCr), Cr component (YCbCr), green component (RGB), Y component (YCbCr), grey component (RGB), red component (RGB), and blue component (RGB) respectively. The separability index achieved for the vision sensor is more than 2.5 times greater than the runner up in the ranking which was the Cb component of colour images. This result confirmed the exceptional capability of the vision sensor to highlight HLB symptoms and differentiate it from HLB-negative and zinc-deficient areas.

The normalised histograms of the symptomatic areas in the images acquired with the vision sensor and top three components of colour images are shown in Fig. 4. In order to conduct a valid comparison, the same symptomatic areas on

Table 3 – Percentage overlap between the histograms of every pair of classes in the images acquired with the vision sensor and top three components of colour images: HLB+ = infected with Huanglongbing; Zn Def. HLB+ = zinc deficient and infected with Huanglongbing; Zn Def. HLB− = zinc deficient but not infected with Huanglongbing; and HLB− = healthy.

Vision sensor				Blue difference (Cb) component of YCbCr			
	HLB+	Zn Def. HLB+	Zn Def. HLB−		HLB+	Zn Def. HLB+	Zn Def. HLB−
HLB−	1.74%	0.00%	0.00%	HLB−	56.21%	1.29%	0.44%
HLB+		11.87%	12.01%	HLB+		14.62%	12.23%
Zn Def. HLB+			80.98%	Zn Def. HLB+			76.05%
Red difference (Cr) component of YCbCr				**Green component of RGB**			
HLB−	22.37%	4.06%	4.07%	HLB−	19.98%	4.92%	1.88%
HLB+		51.66%	46.22%	HLB+		54.75%	38.68%
Zn Def. HLB+			67.36%	Zn Def. HLB+			77.45%

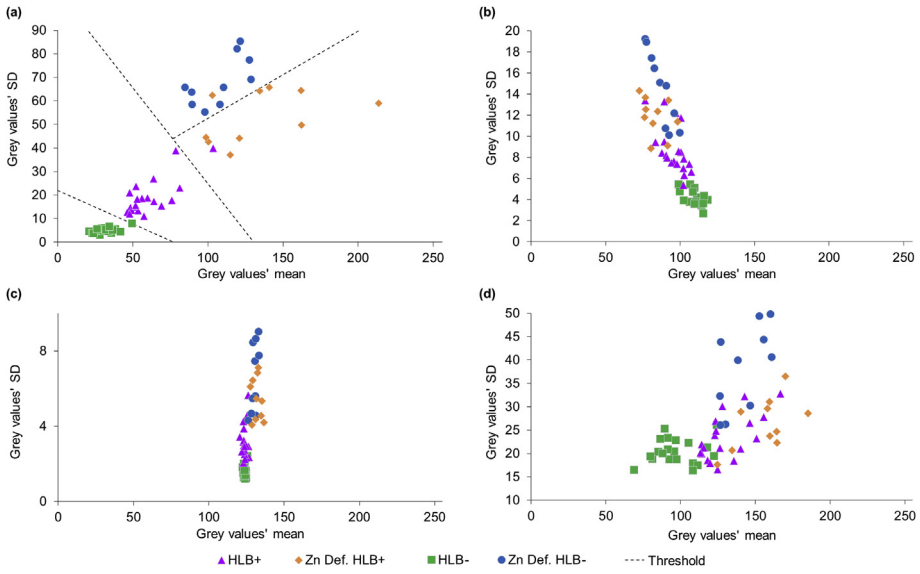

Fig. 5 – Scatter plots of samples in four classes based on their means and standard deviations: (a) vision sensor images, (b) colour images of blue difference (Cb) component of YCbCr, (c) colour images of red difference (Cr) component of YCbCr, (d) colour images of green component of RGB. HLB+ = infected with Huanglongbing, Zn Def. HLB+ = zinc deficient and infected with Huanglongbing, Zn Def. HLB− = zinc deficient but not infected with Huanglongbing, and HLB− = healthy. (For interpretation of the references to colour in this figure legend, the reader is referred to the web version of this article.)

the leaf images were marked and used for creating the histograms. The pixel values belonging to different symptomatic areas were well distributed on the grey scale range (0–255) in the images of the vision sensor, while they are concentrated in limited ranges of grey values for the Cb and Cr components. Table 3 includes the exact overlap percentages between every pair of classes for the vision sensor images and the top three colour images components. Comparing to the colour components, the vision sensor histograms had minimum overlaps between every pair of classes except for the pair of HLB+/HLB− within the zinc deficient class. HLB-negative symptomatic area had zero overlap with zinc deficient classes and only 1.74% overlap with HLB-positive symptomatic areas in the images of the vision sensor while these percentages increased notably for the colour components.

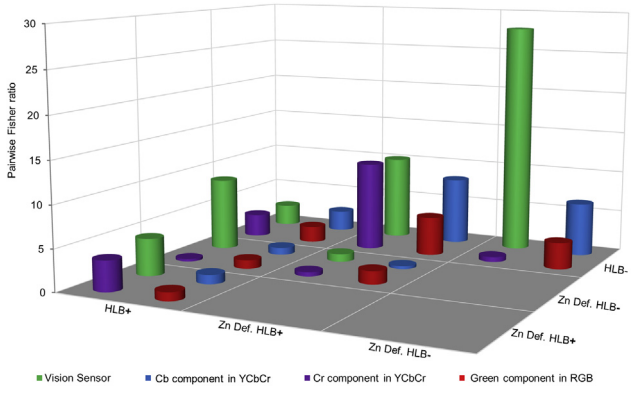

Fig. 6 – Comparison of the pairwise Fisher ratios (as the separability indices) achieved using mean and standard deviation features for the vision sensor and top three colour components: Cb = blue difference (YCbCr), and Cr = red difference (YCbCr).

The scatter plots of leaf areas in the vision sensor and the top three components of the colour images are illustrated in Fig. 5. As the plots suggest, the four classes of leaf samples are more distinctive in the images of the vision sensor compared to the colour image components. The thresholds in the vision sensor scatter plot divided the four classes with maximum possible margin and minimum number of mis-classified samples. In order to find the best thresholds, the maximum margin method was applied in three steps sequentially. At the first step, it determined the optimum threshold between HLB-negative samples and the rest of the dataset. At the second step, the threshold between HLB-positive and zinc-deficient samples was acquired. Finally, at the third step, the best separating threshold between HLB-positive and HLB-negative samples within the zinc-deficient class was obtained. The HLB-negative samples in the vision sensor images had smaller means (from 20 to 50) compared to the other classes. There were neither HLB nor zinc deficiency symptomatic areas on the HLB-negative leaves. Therefore, they reflected the polarised light with the same polarisation planar direction as they were illuminated with and this reflection was filtered by the polarising filter in front of the camera. The means of HLB-negative samples in other colour components, however, were over 68 which usually overlapped with the samples in other classes because the illumination and reflection were not filtered out by the image acquisition process. The HLB-positive samples, on the other hand, had greater means and SDs in the vision sensor scatter plot compared to the HLB-negative samples. Starch accumulation in the HLB-positive samples rotated the polarisation plane of light and, therefore, the symptomatic areas were brighter in the vision sensor images.

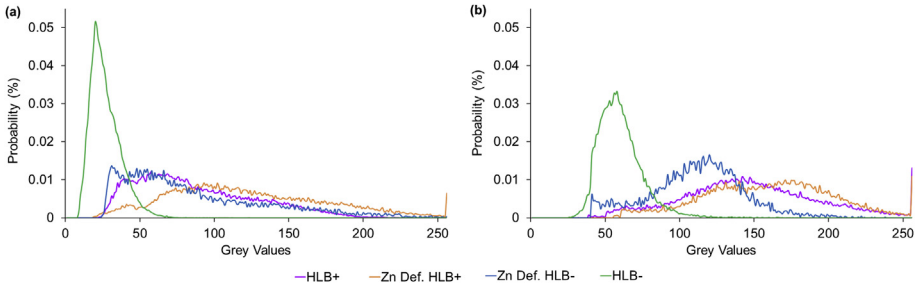

Fig. 7 – Histograms of the entire leaves' areas in four classes (a) before grinding, and (b) after grinding: HLB+ = infected with Huanglongbing; Zn Def. HLB+ = zinc deficient and infected with Huanglongbing; Zn Def. HLB− = zinc deficient but not infected with Huanglongbing; and HLB− = healthy.

The zinc deficiency areas had the brightest pixels in the vision sensor images, while in the other colour components, their pixel values overlapped with other classes. Zinc-deficient leaves contain starch (with different molecular properties from that of HLB-positive leaves) at some level higher than healthy leaves but less than HLB-positive leaves (Gonzalez, Reyes, & Etxeberria, 2011). This might be one explanation for the high pixel values at zinc-deficient symptomatic areas. Within the zinc deficient super class, the HLB-positive samples had greater means and smaller SDs compared to the HLB-negative sample in vision sensor images. The zinc-deficient HLB-positive samples included both zinc deficiency and HLB symptoms so they had larger means. On the other hand, the pixel values belonging to the HLB symptomatic areas (mid-grey pixels) filled the gap between zinc deficient areas (bright pixels) and healthy parts (dark pixels) and as a result, the HLB-positive samples had smaller SDs in the zinc-deficient super class. The zinc-deficient HLB-negative samples had greater SDs in colour components as well, but their means were analogues to the HLB-positive samples which affects the classification accuracy. It can be concluded from the scatter plots in Fig. 5 that the vision sensor provided the best separation between the four classes.

The pairwise Fisher ratios for the vision sensor and the top three components of colour images are illustrated in Fig. 6. Since the dataset included four different classes, a total of six pairwise comparisons were conducted. The vision sensor had better separability indices between the HLB-positive class and both zinc-deficient sub classes as well as between HLB-negative and zinc-deficient HLB-negative classes. The vision sensor and all three colour components presented comparable separability between HLB-positive and HLB-negative classes, still a better separability can be seen in the scatter plot of the vision sensor (Fig. 5). The separability indices between the HLB-positive and HLB-negative classes within the zinc deficient class were relatively smaller compared to the other pairs of classes; while the green component produced slightly better separability than the vision sensor. It is likely that starch in the zinc-deficient HLB-positive samples is more of a mixture of HLB-positive and zinc-deficient properties, which is more difficult to discern.

3.3. *Comparison of sample conditions*

The normalised histograms of the entire leaf areas (not just the symptomatic areas) in the vision sensor images are shown in Fig. 7 before and after grinding and in four different classes. It can be seen in the normalised histograms that the leaf images became brighter after grinding.

In general, the back side of the citrus leaf is brighter than its front side, probably due to the thinner cuticle and more compact epidermis. After grinding, both sides of the leaves were mixed so the ground leaves looked brighter. The histograms of HLB-negative samples were noticeably detectable from the other classes in both plots. The histogram of the HLB-positive samples was comparable to the zinc-deficient HLB-negative class before grinding; but after grinding the HLB-positive samples became brighter. The accumulated starch was more visible after grinding and this could be a reason for more brightness in ground leaf images. According to Fig. 7, zinc-deficient HLB-positive samples were the brightest class both before grinding and after grinding. Including both HLB

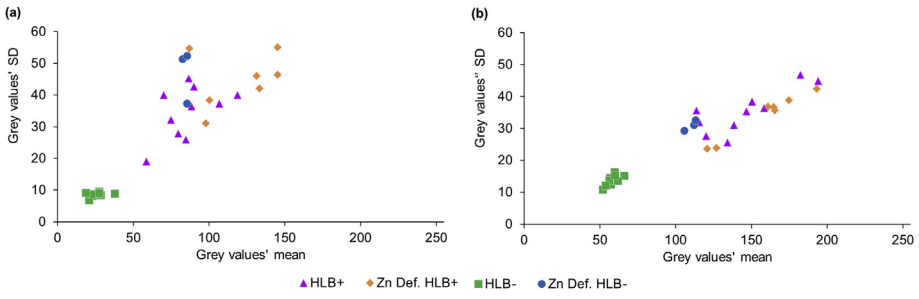

Fig. 8 – Scatter plots of samples in four classes based on their mean and standard deviation (a) before grinding, and (b) after grinding. HLB+ = infected with Huanglongbing, Zn Def. HLB+ = zinc deficient and infected with Huanglongbing, Zn Def. HLB− = zinc deficient but not infected with Huanglongbing, and HLB− = healthy.

and zinc deficiency symptoms made them brighter on average compared to the other classes.

The scatter plots of samples before and after grinding are illustrated in Fig. 8. As the histograms in Fig. 7 also suggest, the grey value means generally increased after grinding but the range of SD variation decreased. Before grinding, the means of the HLB-positive samples were close to the means of the zinc-deficient HLB-negative leaves; however, after being ground their means were more similar to the zinc-deficient HLB-positive samples. This is another reason that supports the unique starch characteristic of rotating the polarisation plane of light and becoming brighter in the images acquired by the vision sensor. Since the samples from both HLB positive and zinc-deficient HLB-positive classes included excessive levels of starch, and their starch content was more visible after being ground, they had more high-intensity pixels and consequently greater grey value means also.

The pairwise Fisher ratios before and after grinding are plotted in Fig. 9. The separability indices (arithmetic averages of Fisher ratios) of 0.415, and 0.559 were achieved for samples before and after being ground, respectively. According to Fig. 9, the HLB-positive and HLB-negative samples were better separated in the ground leaf images, regardless of their zinc deficiency. Again that was due to more visibility of starch after grinding. HLB-positive and zinc-deficient HLB-positive classes were hardly separable after grinding (Fisher ratio < 0.1). On average, the grey value means increased by 72% for HLB-positive samples after grinding, while this percentage was about 32% for zinc deficient samples. One reason might be that HLB symptom overrode zinc deficiency symptom in zinc-deficient HLB-positive ground leaves, and as a result only HLB symptoms could be seen after grinding. On the other hand, the average of grey value SDs increased by 7% for the HLB-positive samples after grinding, while it decreased by 25% for the zinc-deficient leaves. In other words, after grinding the zinc-deficient leaves had smoother images, while there was more contrast in the images of the HLB-positive samples which happened due to the increased difference between the pixel values of HLB symptomatic and healthy areas. This was another proof supporting the outstanding capability of the vision sensor to highlight the starch accumulation in citrus leaf.

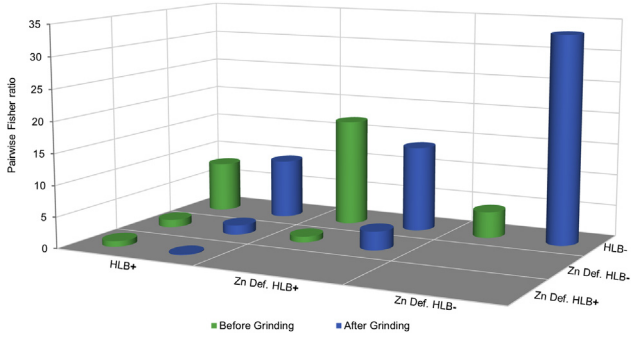

Fig. 9 – The pairwise fisher ratio and arithmetic average of Fisher ratio as the separability index achieved using mean and standard deviation features before and after grinding: HLB+ = infected with Huanglongbing; Zn Def. HLB+ = zinc deficient and infected with Huanglongbing; Zn Def. HLB− = zinc deficient but not infected with Huanglongbing; and HLB− = healthy.

The separability index between the HLB-positive and zinc-deficient HLB-negative samples did not change much after being ground. However, a large increase in the Fisher ratio is apparent for the pair of HLB-negative and zinc-deficient HLB-negative classes which also influenced the increased arithmetic average of the Fisher ratios for ground leaves. It can be concluded that the four classes were generally better separated after grinding; however, the separability before grinding was acceptable enough for a non-destructive on-the-go HLB diagnosis application.

Among different HLB identification approaches, aerial imaging systems can conduct the quickest diagnosis on a large scale grove (Li, Lee, Li, et al., 2012); however, compared to the method introduced in this study, airborne image analysis is less accurate, more costly, and more complicated. The laboratory-based diagnosis methods such as qrt-PCR test (Hansen et al., 2008) and starch measurement (Gonzalez et al., 2012) can perform the most accurate HLB identification; however, these methods can be only conducted in a laboratory, they are time consuming and they need an additional step of sample collection, while the vision sensor in this paper can handle a real-time on-the-go diagnosis. Also it can be easily equipped with a Differential Global Positioning System (DGPS) to produce the HLB status map of the grove.

4. Conclusion

A new prototype vision sensor was introduced in this study which was able to recognise HLB infection with high accuracy. One of the main advantages of this vision sensor was the ability to highlight the symptomatic areas by employing a customised illumination system and proper use of polarising filters. The other important advantage was the non-destructive diagnosis capability of this sensor in which no sample preparation was required. Two experiments were designed to assess these two features of the sensor. The results confirmed that the narrow band polarised illumination at 591 nm significantly increased the diagnosis accuracy. Additionally, it was shown that grinding the citrus leaf samples could increase the separability index; however, the images of unground leaves were informative enough for a non-destructive on-the-go diagnosis application. Another advantage of this sensor was its affordability. This sensor included a few inexpensive components which makes it a reasonably priced approach for every citrus grower. The total cost of the sensor components was less than 1000 US$. This sensor can help growers conduct a constant monitoring of their grove and prevent huge losses from major and incurable HLB infection.

Acknowledgements

The authors would like to thank the Citrus Research and Development Foundation (Project number: 11-124-423) for

funding this project. Additionally, we would like to thank Dr. Reza Ehsani, and Ms. Veronica Campbell at the University of Florida and Mr. Michael Irey at the United States Sugar Corporation, Clewiston, FL for their great support in this study.

REFERENCES

Albrecht, U., & Bowman, K. D. (2008). Gene expression in *citrus sinensis* (L.) osbeck following infection with the bacterial pathogen Candidatus Liberibacter asiaticus causing Huanglongbing in Florida. *Plant Science, 175*(3), 291–306. http://dx.doi.org/10.1016/j.plantsci.2008.05.001.

Bishop, C. M. (2006). *Pattern recognition and machine learning* (1st ed.). New York: Springer Science.

Futch, S., Weingarten, S., & Irey, M. (2009). *Determining HLB infection levels using multiple survey methods in Florida citrus.* Paper presented at the Proc. Fla. State Hort. Soc.

Garcia-Ruiz, F., Sankaran, S., Maja, J. M., Lee, W. S., Rasmussen, J., & Ehsani, R. (2013). Comparison of two aerial imaging platforms for identification of Huanglongbing-infected citrus trees. *Computers and Electronics in Agriculture, 91*(0), 106–115.

Gonzalez, P., Reyes-De-Corcuera, J., & Etxeberria, E. (2012). Characterization of leaf starch from HLB-affected and unaffected-girdled citrus trees. *Physiological and Molecular Plant Pathology, 79*, 71–78. http://dx.doi.org/10.1016/j.pmpp.2012.05.002.

Gonzalez, P., Reyes, J., & Etxeberria, E. (2011). *Starch analysis of HLB-affected and control healthy citrus leaves reveal variations in the amylose/amylopectin ratio.* Paper presented at the Proc. Fla. State Hort. Soc.

Gottwald, T. R. (2010). Current epidemiological understanding of citrus huanglongbing. *Annual Review of Phytopathology, 48*, 119–139. http://dx.doi.org/10.1146/annurev-phyto-073009-114418.

Halbert, S. E. (2005). *The discovery of Huanglongbing in Florida.* Paper presented at the 2nd International Citrus Canker and Huanglongbing Research Workshop, Orlando, Florida.

Han, J.-S., Lee, S. W., & Bien, Z. (2013). Feature subset selection using separability index matrix. *Information Sciences, 223*(0), 102–118. http://dx.doi.org/10.1016/j.ins.2012.09.042.

Hansen, A. K., Trumble, J. T., Stouthamer, R., & Paine, T. D. (2008). A new huanglongbing species,"Candidatus Liberibacter psyllaurous," found to infect tomato and potato, is vectored by the psyllid Bactericera cockerelli (Sulc). *Applied and Environmental Microbiology, 74*(18), 5862–5865.

Hawkins, S. A., Park, B., Poole, G. H., Gottwald, T., Windham, W. R., & Lawrence, K. C. (2010). Detection of citrus huanglongbing by Fourier transform infrared–attenuated total reflection spectroscopy. *Applied Spectroscopy, 64*(1), 100–103.

Kim, D. G., Burks, T. F., Schumann, A. W., Zekri, M., Zhao, X., & Jianwei, Q. (2009). Detection of citrus greening using microscopic imaging. *Agricultural Engineering International: the CIGR Ejournal*. Manuscript 1194. Vol. XI.

Kumagai, L. B., LeVesque, C. S., Blomquist, C. L., Madishetty, K., Guo, Y., Woods, P. W., et al. (2014). First report of Candidatus Liberibacter asiaticus associated with citrus Huanglongbing in California. *Phytopathology, 104*(3), 257–268.

Kunta, M., Sétamou, M., Skaria, M., Rascoe, J., Li, W., Nakhla, M. K., et al. (2012). First report of citrus huanglongbing in Texas. *Phytopathology, 102*, S4.

Li, W., Hartung, J. S., & Levy, L. (2006). Quantitative real-time PCR for detection and identification of Candidatus Liberibacter species associated with citrus huanglongbing. *Journal of Microbiological Methods, 66*(1), 104–115.

Li, X., Lee, W. S., Li, M., Ehsani, R., Mishra, A. R., Yang, C., et al. (2012). Spectral difference analysis and airborne imaging classification for citrus greening infected trees. *Computers and Electronics in Agriculture, 83*, 32–46. http://dx.doi.org/10.1016/j.compag.2012.01.010.

Li, H., Lee, W. S., Wang, R., Ehsani, R., & Yang, C. (2012). *Spectral angle mapper (SAM) based citrus greening disease detection using airborne hyperspectral imaging.* Paper presented at the 11th International Conference on Precision Agriculture. Indianapolis: Indiana.

Li, H., Lee, W. S., Wang, K., Ehsani, R., & Yang, C. (2014). 'Extended spectral angle mapping (ESAM)'for citrus greening disease detection using airborne hyperspectral imaging. *Precision Agriculture, 15*, 162–183.

Mishra, A., Ehsani, R., Albrigo, G., & Lee, W. S. (2007). *Spectral characteristics of citrus greening (Huanglongbing).* Paper presented at the ASABE Annual International Meeting, Minneapolis, Minnesota.

Mishra, A., Karimi, D., Ehsani, R., & Albrigo, L. G. (2011). Evaluation of an active optical sensor for detection of Huanglongbing (HLB) disease. *Biosystems Engineering, 110*, 302–309. http://dx.doi.org/10.1016/j.biosystemseng.2011.09.003.

Pourreza, A., Lee, W. S., Raveh, E., Ehsani, R., & Etxeberria, E. (2014). Citrus huanglongbing disease detection using narrow band imaging and polarized illumination. *Transactions of the ASABE, 57*(1), 259–272.

Pourreza, A., Lee, W. S., Raveh, E., Hong, Y., & Kim, H.-J. (2013). *Identification of citrus greening disease using a visible band image analysis.* Paper presented at the ASABE Annual International Meeting, Kansas City, Missouri http://elibrary.asabe.org/abstract.asp?adid=43724&t=5.

Sankaran, S., Ehsani, R., & Etxeberria, E. (2010). Mid-infrared spectroscopy for detection of Huanglongbing (greening) in citrus leaves. *Talanta, 83*, 574–581. http://dx.doi.org/10.1016/j.talanta.2010.10.008.

Takushi, T., Toyozato, T., Kawano, S., Taba, S., Taba, K., Ooshiro, A., et al. (2007). Scratch method for simple, rapid diagnosis of citrus huanglongbing using iodine to detect high accumulation of starch in the citrus leaves. *Japanese Journal of Phytopathology, 73*.

Texeira, D. C., Ayres, J., Kitajima, E. W., Danet, L., Jagoueix-Eveillard, S., Saillard, C., et al. (2005). First report of a Huanglongbing-like disease of citrus in Sao Paulo State, Brazil and association of a new Liberibacter species,"*Candidatus* Liberibacter americanus", with the disease. *Plant Disease, 89*, 107.

Windham, W. R., Poole, G. H., Park, B., Heitschmidt, G., Hawkins, S. A., Albano, J. P., et al. (2011). Rapid screening of Huanglongbing-infected citrus leaves by near-infrared reflectance spectroscopy. *Transactions of the ASABE, 54*(6), 2253–2258.

Xie, C. Q., Li, X. L., Nie, P. C., & He, Y. (2013). Application of time series hyperspectral imaging (ts-hsi) for determining water content within tea leaves during drying. *Transactions of the ASABE, 56*(6), 1431–1440.